Spurious Modes in Model Order Reduction in Variational Problems in Electromagnetics

Valentín de la Rubia , David Young, Grzegorz Fotyga , *Member, IEEE*, and Michal Mrozowski , *Fellow, IEEE*

Abstract—In this work, we address an everlasting issue in model order reduction (MOR) in electromagnetics that has remained unnoticed until now. Contrary to what has been previously done, we identify for the very first time *spurious modes* in MOR for time-harmonic Maxwell's equations and propose a methodology to remove their negative influence on the reduced order model (ROM) response. These spurious modes have nonzero resonance frequency and may have shown up in the past giving rise to spikes in the frequency response, in effect, deteriorating the accuracy and efficiency of the MOR process. However, they were never characterized as spurious mode contributions, rather they were most likely considered as poor localized approximation issues in the MOR process. When we try to get further physical insights from the ROM, rather than *simple* frequency domain data, we cannot afford any poorly localized approximation issue, that is, any spurious mode in the band of analysis. Otherwise, these mathematical, but nonphysical, modes will mislead the physical behavior of the device under analysis. A computationally inexpensive variational divergence condition is established to identify spurious modes in the band of analysis, since any physical in-band mode must be divergence-free. In addition, once a spurious mode is identified in the band of analysis, its influence is removed from the ROM by a physics-based coupling strategy. As a result, a robust spurious mode contribution-free MOR in electromagnetics is proposed. Finally, several actual microwave circuits, such as a quad-mode filter and a triple-mode triple-band filter, will illustrate the capabilities and efficiency of the proposed approach.

Index Terms—Computer-aided engineering, design automation, finite-element methods, Galerkin method, microwave circuits, reduced basis methods, reduced order systems, spurious modes.

I. INTRODUCTION

SPURIOUS modes have been a long-standing issue in computational electromagnetics (CEM) that nowadays is considered to be solved [1]. Appropriate approximation spaces have paved the way to remove any nonphysical solution from the numerical approximation to time-harmonic Maxwell's equations [2], [3], [4], [5], [6], [7]. However, this issue is still present and special care should be taken whenever additional processing is done on top of any robust spurious-free numerical implementation in CEM. This is indeed the situation in model order reduction (MOR). Spurious modes are mathematical solutions that are nonphysical solutions to a physical problem. These may be the result of not properly imposing the physical model from a mathematical point of view. As a result, additional nonphysical solutions may show up in the mathematical model we are addressing to account for the physics we are interested in. In electromagnetics, spurious modes are solutions that do not satisfy Maxwell's equations, that is, the spurious solutions violate the divergence equations (Gauss' laws), whereas only the curl equations (Ampère's and Faraday's laws) are properly satisfied.

Computer-aided design (CAD) of microwave devices relies on time-consuming electromagnetic simulations, which have to be carried out many times until a target electrical response is obtained. All this turns into a huge computational effort until a given electromagnetic device can satisfy the specifications. Current industrial needs cannot afford this CAD methodology any longer. Different efforts in the CEM community have been carried out to speed this costly process up, and most of them follow the MOR philosophy [8], [9], [10], [11], [12], [13], [14], [15], [16], [17], [18].

A reduced order model (ROM) implies replacing a rather complex physical model with a much simpler mathematical one that still maintains certain physical aspects of the original model within a parameter set. As such, a ROM is *simply* a mathematical model, not a physical one. Thus, spurious modes, which are nonphysical but mathematical solutions, may show up, and we should be extremely cautious about this. It is of paramount importance to prevent the following phenomena.

1) Nonphysical artifacts in the circuit transfer function, the so-called spikes.
2) Distortion in the ROM error estimation, which leads to the oversized ROMs and may considerably affect the overall speed-up in CPU time.
3) Additional in-band eigenresonances may significantly deteriorate any optimization scheme based on the zeros and poles of the circuit transfer function [15].

Spurious modes in MOR in electromagnetics have remained completely unnoticed. Some efforts to remove spurious solutions at low frequency were carried out in [19]. By the same token, using a low-frequency approximation, namely,

neglecting the displacement current, a MOR is proposed that takes into account a Helmholtz decomposition in [20] and [21]. This allows for spurious mode removal since the divergence equations are properly satisfied. We will go back to this important point later in this work. In addition, different localized artifacts in the frequency response of an electromagnetic device were already pointed out in [18] for geometry parametric MOR (PMOR), that is, a ROM where different geometry parameters are taken into account and, as a result, multiple projection bases have to be appended in the PMOR process to account for the different geometries under analysis. In this work, we focus on the analysis of these localized artifacts and show that the spikes in the frequency response are present in any MOR process, including standard fast frequency sweep methodologies, if special care is not taken, and therefore, they are not associated with PMOR using multiple projection bases. As a result, we identify spurious mode solutions in MOR in electromagnetics.

Our starting point draws upon the theoretical analysis of time-harmonic Maxwell's equations, where some frequency-dependent structure is identified. An infinite-dimension state-space dynamical system representation of electromagnetics is discussed, giving rise to a *full-wave* coupling matrix description in electromagnetics, where the port to resonant mode couplings in the structure under analysis can be easily identified [22]. This will be used to properly process the possible spikes in the frequency response. A ROM accounts for the electromagnetics in the band of analysis and, beyond what has been previously done, the appearance of the so-called *spurious* solutions is addressed for the very first time in MOR. Our approach is such that no modification of the original MOR code needs to be carried out, but *only* additional postprocessing is needed to remove any *spurious* contribution from the frequency response. However, a different perspective to the same problem can be proposed, following [23], [24], [25] in a different physics. A mixed variational formulation that properly manages all equations included in time-harmonic Maxwell's equations can be addressed, avoiding any spurious solution.

This work is organized as follows. In Section II, we review the time-harmonic Maxwell's equations in variational form, solve for the electromagnetic field to show their frequency behavior, and detail the infinite dimension state-space dynamical system in electromagnetics. Section III deals with a standard MOR procedure in electromagnetics, details a physical representation of the ROM, and finally shows the issue of spurious modes. In addition, an automatic procedure to filter out any spurious mode contribution in the ROM is discussed. Actual microwave circuits illustrate the capabilities and accuracy of the proposed methodology in Section IV. Finally, we comment on the conclusions in Section V.

II. Problem Statement

The electromagnetic phenomena in a given device are described by Maxwell's equations. Applying the Fourier transform to these, the fields in the transform domain $j\omega$ can be found. They are

$$\nabla \times \mathbf{E} = -j\omega\mu_0\mu_r\mathbf{H} \text{ in } \Omega \tag{1a}$$
$$\nabla \times \mathbf{H} = j\omega\varepsilon_0\varepsilon_r\mathbf{E} \text{ in } \Omega \tag{1b}$$
$$\nabla \cdot (\varepsilon_0\varepsilon_r\mathbf{E}) = 0 \text{ in } \Omega \tag{1c}$$
$$\nabla \cdot (\mu_0\mu_r\mathbf{H}) = 0 \text{ in } \Omega \tag{1d}$$
$$\mathbf{n} \times \mathbf{E} = \mathbf{0} \text{ on } \Gamma_{\text{PEC}} \tag{1e}$$
$$\mathbf{n} \times \mathbf{H} = \mathbf{0} \text{ on } \Gamma_{\text{PMC}} \tag{1f}$$
$$\mathbf{n} \times \mathbf{H} = \mathbf{J} \text{ on } \Gamma \tag{1g}$$

where $\Omega \subset \mathbb{R}^3$ is a source-free sufficiently smooth bounded domain, $\mathbf{n}$ is the unit outward normal vector on the boundary $\partial\Omega$ of Ω, the boundary $\partial\Omega$ of Ω is divided into perfect electric conductor (PEC), perfect magnetic conductor (PMC) and ports, that is, $\partial\Omega = \Gamma_{\text{PEC}} \cup \Gamma_{\text{PMC}} \cup \Gamma$. $\mathbf{E}$ and $\mathbf{H}$ are the electric and magnetic fields, respectively, ε_r and μ_r are, respectively, the relative permittivity and permeability of the medium, which is assumed to be lossless, ε_0 and μ_0 are, respectively, the relative permittivity and permeability of a vacuum, and the tangential field $\mathbf{J}$ is the excitation current at the ports. By the same token, we use the wavenumber, namely, $k = \omega(\mu_0\varepsilon_0)^{1/2}$. Throughout this work, we will indistinctly refer to wavenumber as frequency. Time-harmonic Maxwell's equations can be written in a classical weak formulation over an appropriate admissible function space $\mathcal{H}$, viz.,

$$\text{find } \mathbf{E} \in \mathcal{H} \text{ such that } a(\mathbf{E}, \mathbf{v}) = f(\mathbf{v}) \quad \forall\mathbf{v} \in \mathcal{H}. \tag{2}$$

The bilinear form being

$$a(\mathbf{E}, \mathbf{v}) = \int_\Omega \left(\frac{1}{\mu_r}\nabla \times \mathbf{E} \cdot \nabla \times \mathbf{v} - k^2\varepsilon_r\mathbf{E} \cdot \mathbf{v}\right)dx \tag{3}$$

and the linear form

$$f(\mathbf{v}) = jk\eta_0 \int_{\partial\Omega} \mathbf{J} \cdot \mathbf{v} \, ds = jk\eta_0 \int_\Gamma \mathbf{J} \cdot \mathbf{v} \, ds \tag{4}$$

where η_0 is the intrinsic impedance in a vacuum. Here, the admissible space $\mathcal{H}$ is a subspace in the Hilbert space $H(\text{curl}, \Omega)$ defined by

$$H(\text{curl}, \Omega) = \{\mathbf{u} \in L^2(\Omega, \mathbb{C}^3) \mid \nabla \times \mathbf{u} \in L^2(\Omega, \mathbb{C}^3)\} \tag{5}$$

since $\mathcal{H}$ should take the boundary condition (1e) into account, namely,

$$\mathcal{H} = \{\mathbf{u} \in H(\text{curl}, \Omega) \mid \mathbf{n} \times \mathbf{u} = \mathbf{0} \text{ on } \Gamma_{\text{PEC}}\}. \tag{6}$$

Let us refer to the trace spaces, namely,

$$H^{-\frac{1}{2}}(\text{Div}, \partial\Omega) = \{\mathbf{n} \times \mathbf{u} \text{ on } \partial\Omega \mid \mathbf{u} \in H(\text{curl}, \Omega)\}$$
$$H^{-\frac{1}{2}}(\text{Curl}, \partial\Omega) = \{\mathbf{n} \times \mathbf{u} \times \mathbf{n} \text{ on } \partial\Omega \mid \mathbf{u} \in H(\text{curl}, \Omega)\} \tag{7}$$

and point out that they are dual to each other with the following duality pairing:

$$\langle\mathbf{u}, \mathbf{v}\rangle = \int_{\partial\Omega} \mathbf{u} \cdot \mathbf{v} \, ds \tag{8}$$

$\mathbf{u} \in H^{-\frac{1}{2}}(\text{Div}, \partial\Omega)$ and $\mathbf{v} \in H^{-\frac{1}{2}}(\text{Curl}, \partial\Omega)$. It is now apparent that the excitation current $\mathbf{J}$ belongs to $H^{-\frac{1}{2}}(\text{Div}, \partial\Omega)$.

We refer to [26] and [27] for a thorough explanation of all these spaces.

Following [28], [29], where some frequency structure is shown in the solution to the variational problem (2), we introduce the Helmholtz decomposition

$$\mathcal{H} = \mathcal{H}(\mathrm{curl}0, \Omega) \oplus \mathcal{V} \tag{9}$$

where

$$\mathcal{H}(\mathrm{curl}0, \Omega)$$
$$= \{\mathbf{u} \in \mathcal{H} \mid \nabla \times \mathbf{u} = \mathbf{0}\} \tag{10a}$$
$$\mathcal{V} = \left\{\mathbf{u} \in \mathcal{H} \mid (\varepsilon_r \mathbf{u}, \mathbf{v})_{L^2(\Omega)} = 0 \quad \forall \mathbf{v} \in \mathcal{H}(\mathrm{curl}0, \Omega)\right\} \tag{10b}$$

where $(\cdot, \cdot)_{L^2(\Omega)}$ is the inner product in $L^2(\Omega, \mathbb{C}^3)$. $\mathcal{H}(\mathrm{curl}0, \Omega)$ denotes the nullspace of the curl operator, whereas $\mathcal{V}$ stands for its orthogonal complement within the solution space $\mathcal{H}$ in the following inner product:

$$(\mathbf{u}, \mathbf{v})_{\mu_r, \varepsilon_r} = \left(\frac{1}{\mu_r} \nabla \times \mathbf{u}, \nabla \times \mathbf{v}\right)_{L^2(\Omega)} + (\varepsilon_r \mathbf{u}, \mathbf{v})_{L^2(\Omega)}. \tag{11}$$

It should be noted that both $\mathcal{H}(\mathrm{curl}0, \Omega)$ and $\mathcal{V}$ spaces satisfy the PEC boundary condition on Γ_{PEC}.

The variational problem (2) can be solved by taking into account the following splitting $\mathbf{E} = \mathbf{E}_0 + \mathbf{e}$, $\mathbf{E}_0 \in \mathcal{H}(\mathrm{curl}0, \Omega)$, and $\mathbf{e} \in \mathcal{V}$. We refer to [28] and [29] for the details. As a result, we can make explicit the frequency dependence in the solution to time-harmonic Maxwell's equations (cf. [30], [31])

$$\text{if } k^2 \neq k_n^2, \ \mathbf{E} = \mathbf{E}_0 + \mathbf{e} = \eta_0 \frac{A_0}{jk} \mathbf{e}_0 + jk\eta_0 \sum_{n=1}^{\infty} \frac{A_n}{k_n^2 - k^2} \mathbf{e}_n$$

$$\text{if } k^2 = k_n^2, \ \mathbf{E} = \mathbf{E}_0 + \mathbf{e}$$
$$= \eta_0 \frac{A_0}{jk} \mathbf{e}_0 + jk\eta_0 \sum_{k_n^2 = k^2} \alpha_n \mathbf{e}_n + jk\eta_0 \sum_{k_n^2 \neq k^2} \frac{A_n}{k_n^2 - k^2} \mathbf{e}_n \tag{12}$$

$\mathbf{e}_0 \in \mathcal{H}(\mathrm{curl}0, \Omega)$ is related to the Riesz representative for the electric field in statics and has unit norm. A_0 stands for the coupling coefficient of the excitation current to the static field, namely,

$$A_0 = \langle \mathbf{J}, \mathbf{n} \times \mathbf{e}_0 \times \mathbf{n} \rangle. \tag{13}$$

The set of eigenmodes $\{\mathbf{e}_n \mid n \in \mathbb{N}\} \subset \mathcal{V}$ stands for the resonant modes in electrodynamics, along with their corresponding resonance frequencies k_n and forms a complete orthonormal system in $\mathcal{V}$ with respect to the inner product (11) [28]. It should be pointed out that $\mathcal{H}(\mathrm{curl}0, \Omega)$ is orthogonal to $\mathcal{V}$ with respect to the same inner product (11). Getting to our point, (12) details an orthonormal representation, that is, a Fourier series for the electric field where the frequency dependence is explicit [32]. Furthermore, A_n are coupling coefficients for the excitation current $\mathbf{J}$ to its corresponding resonant mode $\mathbf{e}_n$ and are determined by

$$A_n = k_n^2 \langle \mathbf{J}, \mathbf{n} \times \mathbf{e}_n \times \mathbf{n} \rangle, n \in \mathbb{N}. \tag{14}$$

Finally, α_n are arbitrary coefficients since the electric field is not unique at resonance.

A. State Space Dynamical System Representation in Electromagnetics

Taking a closer look at the electric field representation as a function of frequency detailed in (12), we point out that this representation actually provides a physical description of the electromagnetic phenomena within an orthogonal basis, which includes the eigenmode basis [22]. Indeed, depending on the electric current excitation at the ports $\mathbf{J}$, different modes in the analysis domain may or may not be excited, giving rise to a specific frequency response behavior that stands upon the corresponding resonant modes excited. *No frequency behavior other than the one shown (12) is allowed in electromagnetics.*

An impedance matrix transfer function detailing the input–output behavior of the device under analysis is usually considered. Taking a waveguide mode representation at the ports in the analysis domain for the excitation current $\mathbf{J}$ and the resulting tangential electric field $\mathbf{n} \times \mathbf{E} \times \mathbf{n}$, we get

$$\mathbf{J} = \sum_{p=1}^{M} i_p \mathbf{j}_p = \left(\mathbf{j}_1 \ \cdots \ \mathbf{j}_M\right) \begin{pmatrix} i_1 \\ \vdots \\ i_M \end{pmatrix} \tag{15a}$$

$$\mathbf{n} \times \mathbf{E} \times \mathbf{n} = \sum_{p=1}^{M} v_p \boldsymbol{\epsilon}_p, \text{ on } \Gamma. \tag{15b}$$

The waveguide mode fields $\mathbf{j}_p$ and $\boldsymbol{\epsilon}_q$ satisfy $\langle \mathbf{j}_p, \boldsymbol{\epsilon}_q \rangle = \delta_{pq}$, where δ_{pq} denotes the Kronecker delta. M is the number of waveguide modes at the ports taken into account. i_p and v_p are the input current and output voltage coefficients at the ports, respectively. The output voltage coefficients are determined by

$$\begin{pmatrix} v_1 \\ \vdots \\ v_M \end{pmatrix} = \begin{pmatrix} \langle \mathbf{j}_1, \mathbf{n} \times \mathbf{E} \times \mathbf{n} \rangle \\ \vdots \\ \langle \mathbf{j}_M, \mathbf{n} \times \mathbf{E} \times \mathbf{n} \rangle \end{pmatrix}. \tag{16}$$

Substituting (15a) into the electric field representation (12) yields

$$\text{if } k^2 \neq k_n^2, \ \mathbf{E} = jk\eta_0 \sum_{n=0}^{\infty} \frac{(A_{n1} \ \cdots \ A_{nM})}{k_n^2 - k^2} \mathbf{e}_n \begin{pmatrix} i_1 \\ \vdots \\ i_M \end{pmatrix}$$

$$\text{if } k^2 = k_n^2, \ \mathbf{E} = jk\eta_0 \sum_{k_n^2 = k^2} \alpha_n \mathbf{e}_n$$

$$+ jk\eta_0 \sum_{k_n^2 \neq k^2} \frac{(A_{n1} \ \cdots \ A_{nM})}{k_n^2 - k^2} \mathbf{e}_n \begin{pmatrix} i_1 \\ \vdots \\ i_M \end{pmatrix} \tag{17}$$

where $k_0 := 0$ is the component associated with statics. Once again, α_n are arbitrary coefficients since the electric field is not unique at resonance. The coupling coefficients A_{np} are determined by

$$A_{0p} = \langle \mathbf{j}_p, \mathbf{n} \times \mathbf{e}_0 \times \mathbf{n} \rangle$$
$$A_{np} = k_n^2 \langle \mathbf{j}_p, \mathbf{n} \times \mathbf{e}_n \times \mathbf{n} \rangle, n \in \mathbb{N} \tag{18}$$

which are associated with couplings in statics and eigenresonances, respectively. Finally, putting (16) and (17) together,

we obtain the impedance matrix transfer function, namely

$$
\begin{pmatrix} v_1 \\ \vdots \\ v_M \end{pmatrix} = jk\eta_0 \sum_{n=0}^{\infty} \frac{\begin{pmatrix} a_{n1} \\ \vdots \\ a_{nM} \end{pmatrix} \begin{pmatrix} A_{n1} & \cdots & A_{nM} \end{pmatrix}}{k_n^2 - k^2} \begin{pmatrix} i_1 \\ \vdots \\ i_M \end{pmatrix}
$$
$$
\mathbf{v} = \mathbf{Z}(k)\mathbf{i}. \tag{19}
$$

Coefficients a_{np} are determined by

$$
a_{np} = \langle \mathbf{j}_p, \mathbf{n} \times \mathbf{e}_n \times \mathbf{n} \rangle, n \in \mathbb{N} \cup 0. \tag{20}
$$

The coupling coefficients a_{np} and A_{np} can be conveniently arranged to get a simpler impedance matrix representation (19). Thus,

$$
\begin{pmatrix} v_1 \\ \vdots \\ v_M \end{pmatrix} = jk\eta_0 \sum_{n=0}^{\infty} \frac{\begin{pmatrix} c_{n1} \\ \vdots \\ c_{nM} \end{pmatrix} \begin{pmatrix} c_{n1} & \cdots & c_{nM} \end{pmatrix}}{k_n^2 - k^2} \begin{pmatrix} i_1 \\ \vdots \\ i_M \end{pmatrix}
$$
$$
\mathbf{v} = \mathbf{Z}(k)\mathbf{i} \tag{21}
$$

where the coupling coefficients c_{np} read

$$
\begin{aligned}
c_{0p} &= \langle \mathbf{j}_p, \mathbf{n} \times \mathbf{e}_0 \times \mathbf{n} \rangle \\
c_{np} &= k_n \langle \mathbf{j}_p, \mathbf{n} \times \mathbf{e}_n \times \mathbf{n} \rangle, n \in \mathbb{N}.
\end{aligned} \tag{22}
$$

It is worth noting that the matrix residue for each pole k_n in the impedance matrix transfer function (21) is a rank-1 matrix [22]. This property allows us to rearrange the impedance matrix transfer function in a more suitable way. As a matter of fact, (21) admits a more insightful state-space dynamical system matrix representation, namely

$$
\begin{pmatrix} \mathbf{D} & \mathbf{C} \\ \mathbf{C}^T & \mathbf{A}(k) \end{pmatrix} \begin{pmatrix} \mathbf{i} \\ \mathbf{E} \end{pmatrix} = \begin{pmatrix} \frac{\mathbf{v}}{-jk\eta_0} \\ \mathbf{0} \end{pmatrix} \tag{23a}
$$
$$
\mathbf{v} = jk\eta_0 \left(-\mathbf{D} + \mathbf{C}\mathbf{A}^{-1}(k)\mathbf{C}^T \right)\mathbf{i} = \mathbf{Z}(k)\mathbf{i} \tag{23b}
$$

where $\mathbf{D}$ is an identically zero matrix, $\mathbf{A}(k)$ is a diagonal matrix with entries $k_n^2 - k^2$, namely $\mathbf{A}(k) = \mathbf{K} - k^2\mathbf{Id}$, $\mathbf{K} = \text{diag}\{k_0^2, k_1^2, \ldots\}$,and $\mathbf{Id}$ is the identity matrix, the state-space $\mathbf{E}$ stands for the electric field in the resonant mode basis $\{\mathbf{e}_n, n \in \mathbb{N} \cup 0\}$, and $\mathbf{C}$ matrix entries C_{pn} are already detailed in (22), thus, $C_{pn} = c_{np}$, which stand for the coupling coefficients to each state, that is, to each resonant mode in the analysis domain. As a result, the matrix

$$
\begin{pmatrix} \mathbf{0} & \mathbf{C} \\ \mathbf{C}^T & \mathbf{K} \end{pmatrix} \tag{24}
$$

gives rise to a *full-wave* coupling matrix description of electromagnetics in transversal topology [22], where no approximation is taken into account as it is done in classical coupling matrix circuit theory [33]. No miracle though, the price to pay is that the dynamics in electromagnetics stand upon infinitely many so-called states, that is, resonant modes. MOR will be of help in this regard. We will go back to this point in Section III to remove this limitation.
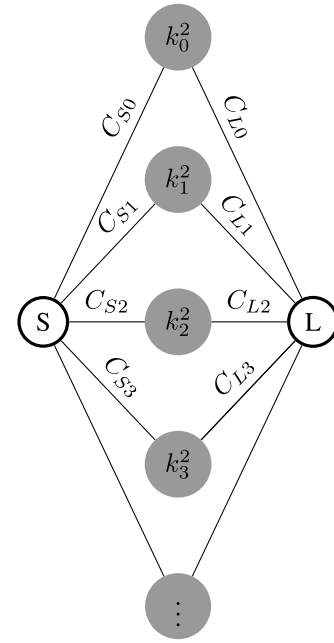

Fig. 1. Transversal topology coupling diagram describing electromagnetics in a two-port device.

Fig. 1 details the coupling diagram for the *full-wave* coupling matrix description of electromagnetics in (24) for a device with two ports, namely S and L (*source* and *load*). The infinitely many states are represented by gray nodes. Nodes are connected to account for electromagnetic coupling. No coupling between states arises since the resonant modes are orthogonal to each other. Recall $\mathbf{K}$ matrix in (24) is a diagonal matrix with entries k_n^2, the resonance frequencies. Only coupling from the ports to the states is allowed, which is detailed in matrix $\mathbf{C}$. As a result, we have a so-called transversal topology coupling matrix with infinitely many states, that is, resonant nodes, which completely describes the physics throughout the whole electromagnetic spectrum, $\forall k \in \mathbb{R}$. All this is detailed in (23) and (24), which is nothing but a state space dynamical system representation of Maxwell's equations. However, a practical representation is needed since we cannot afford to deal with an infinitely many state description of electromagnetics.

III. MODEL ORDER REDUCTION

A ROM replaces a rather complex physical model with a much simpler mathematical one that still maintains certain physical aspects of the original model within a parameter set. The computational complexity of the ROM should be insignificant in contrast to the high computational cost of the original full order model (FOM). MOR has demonstrated its robustness in reducing the complexity of parametric systems [34], [35].

Microwave circuits are designed to perform a target electrical response in a frequency band of interest. Thus, microwave engineers are only focused on this frequency band behavior, rather than the whole electromagnetic spectrum. As a result, a more suitable representation than the one discussed in Section II, namely, a ROM, is possible. However,

special treatment of the original equations should be taken into account for electromagnetics. Unfortunately, this has gone completely unnoticed in the MOR community. In this work, we focus on this *subtle* topic and point out the pitfalls upon which MOR has been traditionally standing in electromagnetics.

Variational formulation to Maxwell's equations (2) turns into a frequency-parameter variational problem, viz.,

$$\text{find } \mathbf{E}(k) \in \mathcal{H} \text{ such that}$$
$$a(\mathbf{E}(k), \mathbf{v}; k) = f(\mathbf{v}; k) \; \forall \mathbf{v} \in \mathcal{H}, \; \forall k \in \mathcal{B} \qquad (25)$$

where $\mathcal{B} = [k_{\min}, k_{\max}]$ is the frequency band of interest, and the frequency-parameter bilinear and linear forms $a(\cdot, \cdot; k)$ and $f(\cdot; k)$ are already defined in (3) and (4), respectively. This time, the frequency dependence on k is highlighted.

The electric field in the frequency band of interest does not arbitrarily vary in the infinite dimension space $\mathcal{H}$. Instead, it evolves on a *simple* manifold induced by the frequency parameter $\mathcal{M}_k = \{\mathbf{E}(k) \in \mathcal{H}, k \in \mathcal{B}\}$, which can be properly approximated by a small dimension projection space $\mathcal{H}_N$. This is where MOR [34], [35] can be of help to quickly find the solution to the frequency-parameter variational problem (25) within a specific tolerance error in a systematic way. For instance, we use the reduced-basis method (RBM) [36], [37] as the MOR procedure. Furthermore, special emphasis has been placed on certifying the accuracy of the ROM in the frequency band of interest $\mathcal{B}$ obtained by the reduced-basis approximation [38], [39], [40], [41], [42]. By the same token, any other MOR scenario can be taken into account in a similar fashion. As a result, the frequency-parameter variational problem (25) turns into a much simpler variational problem, viz.,

$$\text{find } \tilde{\mathbf{E}}(k) \in \mathcal{H}_N \text{ such that}$$
$$a(\tilde{\mathbf{E}}(k), \mathbf{v}; k) = f(\mathbf{v}; k) \; \forall \mathbf{v} \in \mathcal{H}_N, \; \forall k \in \mathcal{B} \qquad (26)$$

where the small dimension projection space $\mathcal{H}_N$ plays the role of the infinite dimension solution space $\mathcal{H}$, $\mathcal{H}_N \subset \mathcal{H}$. The question that remains to be answered is the following: *Does the reduced variational problem* (26) *still provide electromagnetic field solutions to the original variational problem* (25)? The answer is yes and it is straightforward, since all solutions to (25) also satisfy (26), provided the projection space $\mathcal{H}_N$ appropriately approximates the solution manifold $\mathcal{M}_k$. However, we will soon point out that there may be additional solutions to (26) that do not satisfy the original variational problem (25) and, as a result, they are not electromagnetic fields. These will be referred to as *spurious modes*. We will get back to this important point in detail in Section III-A. For the time being, we still follow traditional reasoning.

For the sake of understanding, we use as a projection basis $\mathcal{H}_N$, that is, reduced-basis space to solve problem (26), the in-band eigenmodes enriched by whatever snapshots of the electric field in the frequency band of interest, $\mathbf{E}(\aleph_n)$, $\aleph_n \in \mathcal{B}$, are needed to make the reduced-basis approximation converge to the right solution [29]. However, simpler snapshot-based reduced-basis spaces including moments can be considered [11], [12], [16], [43], [44], [45], [46] and more complicated proper orthogonal decomposition spaces can be

addressed as well [9], [10], [47]. As a result, a *reliable* representation of the electric field in the band of analysis is obtained, namely, $\forall k \in \mathcal{B}$

$$\text{if } k^2 \neq k_n^2, \; \mathbf{E} = jk\eta_0 \sum_{k_n^2 \in \mathcal{B}_2} \frac{A_n}{k_n^2 - k^2} \mathbf{e}_n + \sum_{n=1}^{N} \beta_n(k) \mathbf{E}(\aleph_n)$$

$$\text{if } k^2 = k_n^2 \in \mathcal{B}_2, \; \mathbf{E} = jk\eta_0 \sum_{k_n^2 = k^2} \alpha_n \mathbf{e}_n + \sum_{n=1}^{N} \beta_n(k) \mathbf{E}(\aleph_n)$$
$$(27)$$

where $\mathcal{B}_2$ stands for $[k_{\min}^2, k_{\max}^2]$. Coefficients A_n and $\beta_n(k)$ are conveniently determined by the reduced-basis approximation of problem (25) and can be computed with ease using the reduced-basis space $\mathcal{H}_N = \text{span}\{\mathbf{e}_n, k_n^2 \in \mathcal{B}_2\} + \text{span}\{\mathbf{E}(\aleph_n), \aleph_n \in \mathcal{B}\}$, as has been detailed earlier.

In an analogous way as in Section II, the field solution (27) yields the following impedance matrix transfer function describing electromagnetics, but this time, *only* in the band of interest $\mathcal{B}$. This is the main reason for its simplicity in contrast to (21). Thus,

$$\begin{pmatrix} v_1 \\ \vdots \\ v_M \end{pmatrix} = jk\eta_0 \sum_{k_n^2 \in \mathcal{B}_2} \frac{\begin{pmatrix} c_{n1} \\ \vdots \\ c_{nM} \end{pmatrix} (c_{n1} \cdots c_{nM})}{k_n^2 - k^2} \begin{pmatrix} i_1 \\ \vdots \\ i_M \end{pmatrix}$$

$$+ \mathbf{Z}_{\text{out-of-band}}(k) \begin{pmatrix} i_1 \\ \vdots \\ i_M \end{pmatrix}$$

$$\mathbf{v} = \mathbf{Z}(k)\mathbf{i} = (\mathbf{Z}_{\text{in-band}}(k) + \mathbf{Z}_{\text{out-of-band}}(k))\mathbf{i}. \quad (28)$$

See (21) and (22). It should be pointed out that only in-band modes are considered in $\mathbf{Z}_{\text{in-band}}$, whereas all the out-of-band contribution in $\mathcal{B}$ is put together under $\mathbf{Z}_{\text{out-of-band}}$. However, both terms are finite, no infinitely many terms are taken into account any longer. By the same token, the poles k_n in $\mathbf{Z}_{\text{in-band}}$, that is, the resonances for the resonant modes found in the frequency band of analysis, have rank-1 matrix residues (cf. (28)). Once again, this property allows us to find a more insightful state-space dynamical system matrix representation for $\mathbf{Z}_{\text{in-band}}$. As regards the poles in $\mathbf{Z}_{\text{out-of-band}}$, which are not even physical resonances, but pure mathematical artifacts to account for the in-band contribution from the infinitely many out-of-band modes by means of a *simple* matrix-valued rational function, namely $\mathbf{Z}_{\text{out-of-band}}$, only the physics prevents these poles from appearing in the band of analysis $\mathcal{B}$. We should expect these mathematical artifacts to be out of this band $\mathcal{B}$, but as it will become clear in Section III-A, nothing is done to ensure this physical behavior. As a result, there may be mathematical artifacts in the band of analysis, the so-called *spurious modes* ϵ_n, with resonance frequency $\chi_n \in \mathcal{B}$, whose poles once again show a rank-1 matrix residue property. Taking into account the spurious mode contribution, $\mathbf{Z}_{\text{out-of-band}}$ is split into $\mathcal{Z}_{\text{spurious}}$ and $\mathcal{Z}_{\text{out-of-band}}$. Normally, $\mathcal{Z}_{\text{spurious}}$ should be zero but, as has been previously discussed, this unwanted spurious term may show up if special care is

not taken into account in the MOR process. As a result, (28) turns into

$$
\begin{pmatrix} v_1 \\ \vdots \\ v_M \end{pmatrix} = jk\eta_0 \sum_{k_n^2 \in \mathcal{B}_2} \frac{\begin{pmatrix} c_{n1} \\ \vdots \\ c_{nM} \end{pmatrix} (c_{n1} \cdots c_{nM})}{k_n^2 - k^2} \begin{pmatrix} i_1 \\ \vdots \\ i_M \end{pmatrix}
$$

$$
+ jk\eta_0 \sum_{\chi_n^2 \in \mathcal{B}_2} \frac{\begin{pmatrix} c_{n1} \\ \vdots \\ c_{nM} \end{pmatrix} (c_{n1} \cdots c_{nM})}{\chi_n^2 - k^2} \begin{pmatrix} i_1 \\ \vdots \\ i_M \end{pmatrix}
$$

$$
+ \mathcal{Z}_{\text{out-of-band}}(k) \begin{pmatrix} i_1 \\ \vdots \\ i_M \end{pmatrix}
$$

$$
\mathbf{v} = \mathbf{Z}(k)\mathbf{i}
$$
$$
= \big(\mathbf{Z}_{\text{in-band}}(k) + \mathcal{Z}_{\text{spurious}}(k) + \mathcal{Z}_{\text{out-of-band}}(k)\big)\mathbf{i}. \tag{29}
$$

Recall that the spurious modes arise in the band of analysis $\mathcal{B}$. As result, a more insightful dynamical system matrix representation for the in-band behavior $\mathbf{Z}_{\text{in-band}} + \mathcal{Z}_{\text{spurious}}$ reads

$$
\begin{pmatrix} \mathbf{D} & \mathbf{C} \\ \mathbf{C}^T & \mathbf{A}(k) \end{pmatrix} \begin{pmatrix} \mathbf{i} \\ \tilde{\mathbf{E}} \end{pmatrix} = \begin{pmatrix} \frac{\mathbf{v}}{-jk\eta_0} \\ \mathbf{0} \end{pmatrix} \tag{30a}
$$
$$
\mathbf{v} = jk\eta_0\big(-\mathbf{D} + \mathbf{C}\mathbf{A}^{-1}(k)\mathbf{C}^T\big)\mathbf{i}
$$
$$
= \big(\mathbf{Z}_{\text{in-band}}(k) + \mathcal{Z}_{\text{spurious}}(k)\big)\mathbf{i} \tag{30b}
$$

where $\mathbf{D}$ is an identically zero matrix, $\mathbf{A}(k)$ is a diagonal matrix with entries $k_n^2 - k^2$ and $\chi_n^2 - k^2$, namely, $\mathbf{A}(k) = \mathbf{K} - k^2\mathbf{Id}$, $\mathbf{K} = \text{diag}\{k_n^2 \in \mathcal{B}_2\} \cup \{\chi_n^2 \in \mathcal{B}_2\}$, the state-space $\tilde{\mathbf{E}}$ stands for the electric field in the in-band resonant mode and the spurious mode basis $\{\mathbf{e}_n, k_n^2 \in \mathcal{B}_2\} \cup \{\boldsymbol{\epsilon}_n, \chi_n^2 \in \mathcal{B}_2\}$, and $\mathbf{C}$ matrix entries C_{pn}, detailed in (22) ($C_{pn} = c_{np}$), stand for the coupling coefficients to each in-band state, including the spurious modes. This time, all matrices in the dynamical system are finite. See (23) and (24). As a result, the finite matrix

$$
\begin{pmatrix} \mathbf{0} & \mathbf{C} \\ \mathbf{C}^T & \mathbf{K} \end{pmatrix} \tag{31}
$$

gives rise to a *full-wave* coupling matrix in transversal topology describing electromagnetics in the band of interest $\mathcal{B}$.

Putting everything together, that is, $\mathbf{Z}_{\text{in-band}}$, $\mathcal{Z}_{\text{spurious}}$, and $\mathcal{Z}_{\text{out-of-band}}$, we have the big picture shown in Fig. 2(a) for a two-port device. In contrast to what is detailed in Fig. 1 for the same device, a more compact representation is obtained in Fig. 2(a). However, spurious modes shown as red nodes in the diagram may appear in the ROM. The coupling to these spurious modes is weak since they should not have any influence on the electromagnetic behavior of the microwave device. However, their appearance does interfere with the circuit response, creating some unwanted spikes around the spurious mode resonance frequencies. As a result, their influence should be completely filtered out from the
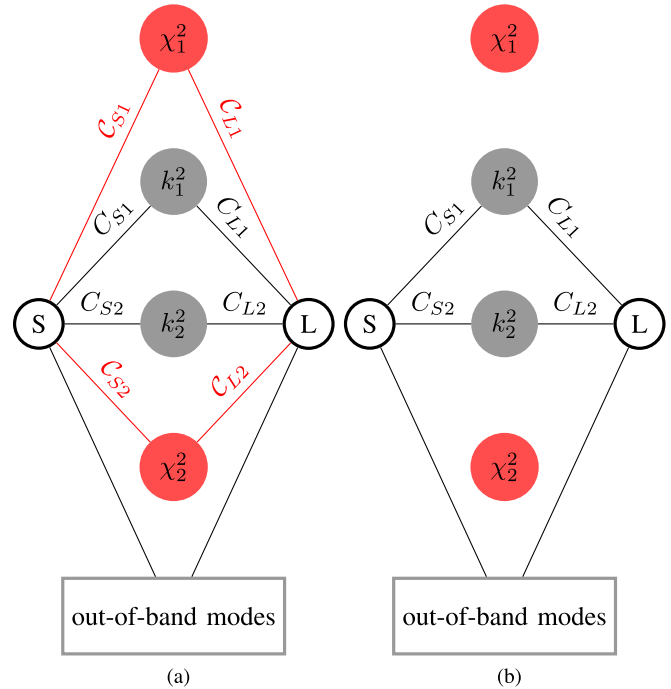

Fig. 2. Transversal topology coupling diagram describing electromagnetics in a two-port device. (a) Spurious mode influence. (b) No spurious mode influence.

circuit response. In this *full-wave* transversal coupling matrix setting, this can be carried out with ease in a process that we call regularization. It is enough to nullify the coupling coefficients C_{pn} from the ports to the spurious resonances in order to avoid this unwanted spurious mode influence in the microwave circuit response. This is shown in Fig. 2(b).

For the sake of understanding, we detail next the coupling matrix (31) for the two-port device shown in Fig. 2(a)

$$
\begin{pmatrix} 0 & 0 & \mathcal{C}_{S1} & C_{S1} & C_{S2} & \mathcal{C}_{S2} \\ 0 & 0 & \mathcal{C}_{L1} & C_{L1} & C_{L2} & \mathcal{C}_{L2} \\ \mathcal{C}_{S1} & \mathcal{C}_{L1} & \chi_1^2 & 0 & 0 & 0 \\ C_{S1} & C_{L1} & 0 & k_1^2 & 0 & 0 \\ C_{S2} & C_{L2} & 0 & 0 & k_2^2 & 0 \\ \mathcal{C}_{S2} & \mathcal{C}_{L2} & 0 & 0 & 0 & \chi_2^2 \end{pmatrix} \tag{32}
$$

as well as the coupling matrix where any influence from the spurious modes is filtered out from the electromagnetic response, as shown in Fig. 2(b), thus

$$
\begin{pmatrix} 0 & 0 & \mathbf{0} & C_{S1} & C_{S2} & \mathbf{0} \\ 0 & 0 & \mathbf{0} & C_{L1} & C_{L2} & \mathbf{0} \\ \mathbf{0} & \mathbf{0} & \chi_1^2 & 0 & 0 & 0 \\ C_{S1} & C_{L1} & 0 & k_1^2 & 0 & 0 \\ C_{S2} & C_{L2} & 0 & 0 & k_2^2 & 0 \\ \mathbf{0} & \mathbf{0} & 0 & 0 & 0 & \chi_2^2 \end{pmatrix}. \tag{33}
$$

Remark 1: It should be pointed out that no coupling between the in-band states arises, only coupling from the ports to each in-band mode is allowed, which is also detailed in Fig. 2 by means of connected nodes.

Remark 2: The out-of-band contribution $\mathcal{Z}_{\text{out-of-band}}$ is not neglected at any point in the analysis. The coupling matrix response is not enough to account for electromagnetics in the

band of analysis $\mathcal{B}$. In other words, the out-of-band eigenmode contribution cannot be neglected from the electromagnetic response. These higher-order modes are indeed contributing to electromagnetics and must be taken into account. As a result, the coupling matrix results themselves do not stand alone to account for the electromagnetic behavior of the device under analysis, but higher-order mode contributions must be considered within the out-of-band contribution $\mathcal{Z}_{\text{out-of-band}}$.

A. Spurious Modes

The appearance of the so-called spurious modes in MOR in electromagnetics still needs to be justified. These spurious mode solutions have remained unnoticed most probably due to the fact that whenever artificial spikes in the frequency response of an electromagnetic device were found by the ROM, the projection space was enriched to actually get rid of these unwanted artifacts by pushing them out of the band. However, spurious modes do appear in the MOR response and special treatment should be carried out if we do not wish to pay the costly price of oversampling to avoid their appearance in the frequency band of analysis $\mathcal{B}$. We mention oversampling since you can always get rid of these spikes in the frequency response by sampling the FOM at these spike frequencies and artificially increasing the order of your ROM. These artifacts were already reported in [18] for geometry PMOR; however, these spurious modes are inherent to any MOR in electromagnetics if special care is not taken.

The main question here is whether the reduced frequency-parameter variational problem (26) satisfies the time-harmonic Maxwell's equations (1) in the band of interest $\mathcal{B}$, such as it is the case for the original frequency-parameter variational problem in (25). The *only* thing that is changed in both variational problems is the admissible solution space. In the original problem (25), an infinite dimension space $\mathcal{H}$ is used, whereas a small dimension projection space $\mathcal{H}_N$ is considered in the reduced problem (26) instead. It should be highlighted that $\mathcal{H}$ is an infinite dimension space and, as a result, the variational problem (25) is completely equivalent to Maxwell's equations in (1) in the strong sense. Note that by taking the divergence in (1a) and (1b), we automatically obtain the divergence equations (1c) and (1d). This is the reason why, in the *continuous* level, only the curl equations [Ampère's and Faraday's laws (1a) and (1b)] are needed to impose the divergence equations (1c) and (1d), provided the frequency ω does not vanish. Up to now, the answer was clear and nobody has reported any issue with MOR in electromagnetics. However, taking a closer look at the time-harmonic Maxwell's equations, we realize that the divergence-free equation (1c) is not accurately taken into account in (26). This is in contrast to what is done in (25), where the divergence-free equation is properly imposed in a variational sense by means of the infinite dimension $\mathcal{H}$ as has been already pointed out, that is,

$$(\varepsilon_r \mathbf{u}, \mathbf{v})_{L^2(\Omega)} = 0 \ \forall \mathbf{v} \in \mathcal{H}(\text{curl0}, \Omega) \tag{34}$$

is a variational equivalence to the divergence-free equation $\nabla \cdot (\varepsilon_r \mathbf{u}) = 0$. The infinite dimension space $\mathcal{H}(\text{curl0}, \Omega)$

is replaced in (26) by a rather small dimension reduced-basis space, even smaller than the dimension of the projection space $\mathcal{H}_N$. As a matter of fact, (34) turns into

$$(\varepsilon_r \mathbf{u}, \mathbf{v})_{L^2(\Omega)} = 0 \ \forall \mathbf{v} \in \mathcal{H}_N(\text{curl0}, \Omega) \tag{35}$$

in the reduced variational problem (26), which unfortunately is not enough to accurately impose the divergence-free equation (1c) in the time-harmonic Maxwell's equations. In other words, the curl equations (1a) and (1b) are not satisfied in the strong sense, and these are *only* satisfied in the weak sense (variational sense in an approximation space of low dimension). This does not allow us to take the divergence operator in the strong sense, just like we have done above, to satisfy the divergence equations (1c) and (1d), provided the frequency ω does not vanish. This is the rationale behind the divergence equations are not imposed in MOR in electromagnetics in (26). As a result, spurious mode solutions with a nonvanishing divergence are expected in the ROM. These are mathematical solutions to (26) that do not satisfy Maxwell's equations and should be conveniently removed from the electromagnetic spectrum, since they do not account for electromagnetics. The way to filter out their contribution from the microwave circuit response has already been discussed in Section III. The question that still remains is how to efficiently identify these spurious modes in the MOR setting, so that their negative influence on the circuit response can be properly removed, regularizing the ROM. Algorithm 1 is proposed to carry out a reliable MOR process that automatically removes any spurious mode contribution, where no *a priori* knowledge of the in-band resonant modes is taken into account as it is the case in [16] and [29], which may be time-consuming depending on the scenario.

Remark 3: It should be pointed out that the rationale for spurious modes in electromagnetics to appear is the divergence-free equation being not properly satisfied. As a result, additional mathematical solutions, which are nonphysical, show up as spurious eigenmodes. Since these spurious modes do not account for electromagnetics, a weak coupling to the excitation ports in the structure under analysis should be expected. This is a direct consequence of being a nonphysical eigenmode. We have taken advantage of this fact to propose Algorithm 1 and filter out any spurious contribution from the frequency response without having to modify the MOR code.

Remark 4: These spurious mode solutions are well known in CEM [1], [5], [6]. They appear whenever a proper finite-element approximation space $\mathcal{H}^h$ to the infinite dimension solution space $\mathcal{H}$ is not taken into account. Nédélec finite elements [2], [3] provide an elegant way to impose the variational divergence-free condition in (34) by means of a sufficiently large finite dimension space $\mathcal{H}^h(\text{curl0}, \Omega)$, which is directly contained in the finite-element space $\mathcal{H}^h$. However, we cannot afford large dimension projection spaces in MOR; otherwise, we deviate from the main goal in a ROM, which should definitely be of small dimension and quick to evaluate. A spurious-free variational formulation for MOR in electromagnetics is currently under investigation and we intend to report these results in the near future.

Remark 5: In order to appropriately compute the variational divergence norm in Step 7 in Algorithm 1, a tree–cotree splitting of the finite-element approximation space is carried out [7], [48], giving rise to a discrete Helmholtz decomposition of the finite-element space. This allows us to appropriately identify the curl-free space in the finite-element approximation. By the same token, a fast evaluation of the variational divergence norm is needed throughout the band of analysis $\mathcal{B}$. This can be straightforwardly computed in a similar fashion as the residual error norm in Step 16, taking advantage of the affine parameter dependence in the ROM [42], [44], [49]. Further details about the norm in a dual space can be found in [50]. In any case, since the solution takes place in a discrete setting, any norm can actually be taken into account to measure the relevance of the divergence of the eigenmodes. No matter which norm is used in this numerical computation, the evaluation of the norm of the divergence of the eigenmode, whatever it is finally used, is computationally cheap by following a similar procedure as the one used in the residual error norm in Step 16.

Remark 6: The rank-1 matrix residue property for each in-band eigenmode, including spurious modes, is double-checked in Step 9. This allows us to identify when an eigenmode is accurately approximated in the MOR procedure [51].

Remark 7: Even though it can be thought that spurious mode identification can actually be accomplished by simply looking at the coupling of these modes to the ports, which should be expected to be weak since they do not account for electromagnetics, this is not enough to properly identify the appearance of such unwanted nonphysical modes. In fact, in the structure under analysis, we can also have physical eigenmodes with a really weak coupling to the excitation ports and, therefore, we cannot only use this criterion to identify the spurious solutions. For instance, this situation can happen in a filter with a small first coupling iris to the cavity modes. These eigenmodes are physical but show a really weak coupling to the ports.

Remark 8: In Step 4 in Algorithm 1, we refer to the eigenproblem resulting from (26) when no excitation is taken into account. It should be noted that the bilinear and linear forms in (26) are defined in (3) and (4). As a result, the eigenproblem coming from (26) turns into matrix form as follows:

$$(\mathbf{S} - k^2\mathbf{T})\mathbf{x} = \mathbf{0} \tag{36}$$

and matrices $\mathbf{S}$ and $\mathbf{T}$ are the ones to diagonalize.

Remark 9: Any physical mode must satisfy Maxwell's equations. As a result, any physical mode is divergence-free, even if it shows a weak coupling to the excitation ports. By the same token, any eigenmode, even if it is a physical or spurious mode, must satisfy the rank-1 matrix residue property. The rationale behind this is being an eigenmode. See (29) and the derivations that brought this equation up.

Remark 10: It should be pointed out that there are some scenarios that, even when spurious modes are present, their negative influence will not show up on the frequency axis and the spurious solution can remain unnoticed. This is the case in open problems such as radiation problems, or lossy problems.

Algorithm 1 Reliable MOR Procedure to Automatically Filter Out the Spurious Mode Contributions

---

Input: Frequency band of interest $\mathcal{B} := [k_{\min}, k_{\max}]$, tolerance `tol` as the acceptable ROM error, and divergence tolerance `tol`$_{\text{div}}$ as divergence-free threshold.

Output: Spurious mode contribution-free ROM.

1: Initialize $\mathcal{H}_N = \{\mathbf{0}\}$, $\xi = $ `tol` $+ 1$. Choose a sample k^* taken from $\mathcal{B}$.

2: **while** $\xi > $ `tol` **do**

3:    Solve for $\mathbf{E}(k^*)$ in (25) and update $\mathcal{H}_N$: $\mathcal{H}_N = \mathcal{H}_N + \text{span}\{\mathbf{E}(k^*)\}$.

4:    Using $\mathcal{H}_N$, solve for the eigenvalue problem in (26) and diagonalize it.

5:    Find the in-band eigenvalues and form the dynamical system (30).

6:    **for** each in-band eigenmode $\mathbf{e}_n$ **do**

7:       Compute the variational divergence norm

$$\texttt{div} = \|\nabla \cdot (\varepsilon_r \mathbf{e}_n)\|_{\mathcal{H}'(\text{curl}0, \Omega)}.$$

   Here

$$\|\nabla \cdot (\varepsilon_r \mathbf{e}_n)\|_{\mathcal{H}'(\text{curl}0, \Omega)} := \sup_{\mathbf{v} \in \mathcal{H}(\text{curl}0, \Omega)} \frac{(\varepsilon_r \mathbf{e}_n, \mathbf{v})_{L^2(\Omega)}}{\|\mathbf{v}\|_{L^2(\Omega)}}.$$

8:       Compute the matrix residue $\mathbf{R}_n$ associated with $\mathbf{e}_n$.

9:       **if** rank$(\mathbf{R}_n)$ $== 1$ and div $>$ `tol`$_{\text{div}}$ **then**

10:          Mark as spurious mode.

11:          Update the dynamical system (30) by removing this spurious mode contribution, nullifying its coupling to the ports.

12:       **end if**

13:    **end for**

14:    Solve for $\tilde{\mathbf{E}}(k)$ in the spurious mode contribution-free diagonal version of (26).

15:    Other MOR processes are possible but, using RBM, choose the next sample k^* from $\mathcal{B}$ as

$$k^* = \arg \max_{k \in \mathcal{B}} \|r(\tilde{\mathbf{E}}(k), \cdot; k)\|_{\mathcal{H}'}.$$

   Here $r(\tilde{\mathbf{E}}(k), \cdot; k)$ is the residual functional introduced by $\tilde{\mathbf{E}}(k)$ in (25), namely,

$$r(\tilde{\mathbf{E}}(k), \cdot; k) := f(\mathbf{v}; k) - a(\tilde{\mathbf{E}}(k), \mathbf{v}; k), \forall \mathbf{v} \in \mathcal{H}.$$

16:    $\xi = \|r(\tilde{\mathbf{E}}(k^*), \cdot; k^*)\|_{\mathcal{H}'}.$

17: **end while**

Spurious modes in MOR may show up in the traditional framework, since the divergence-free equation is not properly imposed. Nevertheless, in these lossy problems, the resonances are no longer found on the frequency axis but they are away from the frequency axis.

IV. NUMERICAL RESULTS

In this section, we apply the proposed methodology to find a spurious mode contribution-free ROM in time-harmonic Maxwell's equations. These kinds of ROMs without spurious

mode contribution are of paramount importance in getting physical insights from MOR in electromagnetics [22], where spurious modes can definitely mislead the physical behavior description of the device under analysis. By the same token, whenever PMOR is taken into account, the projection basis is rich enough to accurately approximate the solution state for the actual device parameter analysis, but also is large enough to account for other analyses in the parameter set of interest. This will definitely find spurious modes in the band of analysis, which must be conveniently removed from the ROM to avoid spikes in the frequency response of the device under analysis. This unwanted behavior has already been pointed out in [18] for geometry PMOR. Algorithm 1 can appropriately take care of these spurious modes in all these scenarios.

The proposed approach is applied to actual microwave circuits, namely, a quad-mode dielectric resonator filter, a triple-band filter in elliptical cavities, and an inline dielectric resonator filter with finite transmission zeros. No loss is taken into account in these circuits under analysis. The operating frequency band is typical for the analysis of these filtering structures. We use RBM [36], [37] as MOR procedure. Throughout these examples, we follow Algorithm 1 to get no spurious contribution in the frequency response of the devices under analysis. We run the MOR procedure with $\mathtt{tol} = 10^{-8}$ as acceptable error, following the tolerance error detailed in [29], where a linear independence measure threshold is used to monitor the accuracy of the ROM. This allows the MOR procedure to automatically stop whenever this error tolerance $\mathtt{tol}$ is ensured, giving rise to a specific order in the ROM, which is adaptively and automatically chosen by Algorithm 1. By the same token, we set $\mathtt{tol_{div}} = 10^{-12}$ to ensure that the divergence-free condition is held, where the value is chosen to account for numerically zero divergence values. The capabilities and reliability of the proposed procedure will be apparent throughout these examples. The in-house C++ code for FEM simulations uses a second-order first family of Nédélec's elements [2], [52], on meshes provided by Gmsh [53]. All computations were carried out on a workstation with a 3.00-GHz Intel Xeon E5-2687W v4 processor and 256-GB RAM.

A. Quad-Mode Dielectric Resonator Filter

A quad-mode dielectric resonator filter in a single cylindrical cavity is proposed in [54]. Fig. 3 shows the geometry of the filter as well as the mesh used for its analysis. These structures are extremely attractive since multiple resonant modes show up in a single cylindrical cavity due to the dielectric resonator. A wide-band analysis is carried out to check for higher-frequency pass bands, $\mathcal{B} := [3.4, 4.5]$ GHz.

An FEM system with 245 778 degrees of freedom is used to solve for the electric field in the band of interest $\mathcal{B}$. Following Algorithm 1, a ROM is obtained by means of RBM giving rise to a reduced system of dimension 14 to compute the frequency response detailed in Fig. 4(a). It should be pointed out that all steps in Algorithm 1 are run until the final dimension 14 to ensure the convergence of the ROM is obtained. No spurious mode was previously identified in this process. By the same
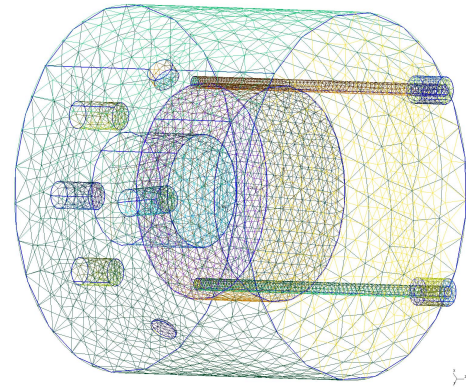

Fig. 3.   Quad-mode dielectric resonator filter proposed in [54].

token, it is guaranteed that this ROM is indeed a surrogate of the FEM model [11], [29], [38], [43], [46]. The comparison between the FEM and MOR results is depicted in Fig. 4. The in-band modes found in the band of analysis are also detailed along the frequency axis in Fig. 4(a). It is clear that finding the eigenvalues in the ROM system of dimension 14 is completely straightforward in contrast to the eigenvalues of the FOM system of dimension 245 778. Furthermore, we find a spike in the scattering parameter response around 4.372 GHz. We may think this spike is indeed due to the actual physical behavior of the quad-mode filter. However, when we carry out the variational divergence analysis for each of the in-band modes, shown in Fig. 4(b), we realize this spike is due to a spurious mode solution, that is, a nonphysical mode, since it does not show a divergence-free contribution as can be observed in the remaining in-band modes. As a result, this spurious mode contribution should be removed from the device response. This is done by means of the methodology detailed in Section III and the results are presented in Fig. 4(c). This time, no spike is observed in the scattering parameter response since any spurious mode contribution has been filtered out in Fig. 4(c) and good agreement is found with respect to the previous spurious mode contribution response in Fig. 4(a).

B. Elliptical-Cavity Triple-Band Filter

A compact triple-band filter with elliptical cavities is detailed in Fig. 5. This filter is proposed in [55]. The elliptical cavities are designed to realize triple-mode resonators, thus significantly reducing the actual size of the triple-band filter. The 3.7–4.4 GHz band is taken into account for analysis. An FEM discretization shown in Fig. 5 with 311 898 degrees of freedom is used. Algorithm 1 is run to carry out a spurious mode contribution-free reliable fast frequency sweep of the triple-band filter. A ROM of dimension 13 is obtained. The scattering parameters are depicted in Fig. 6(d) and the in-band modes are detailed along the frequency axis. The comparison between the FEM and MOR results is depicted in Fig. 6(d) as well and good agreement is found. However, in order to get further insights about this proposed approach, we show the results, following Algorithm 1, for the ROM of dimension 12 in Fig. 6(a), where the in-band modes are depicted as
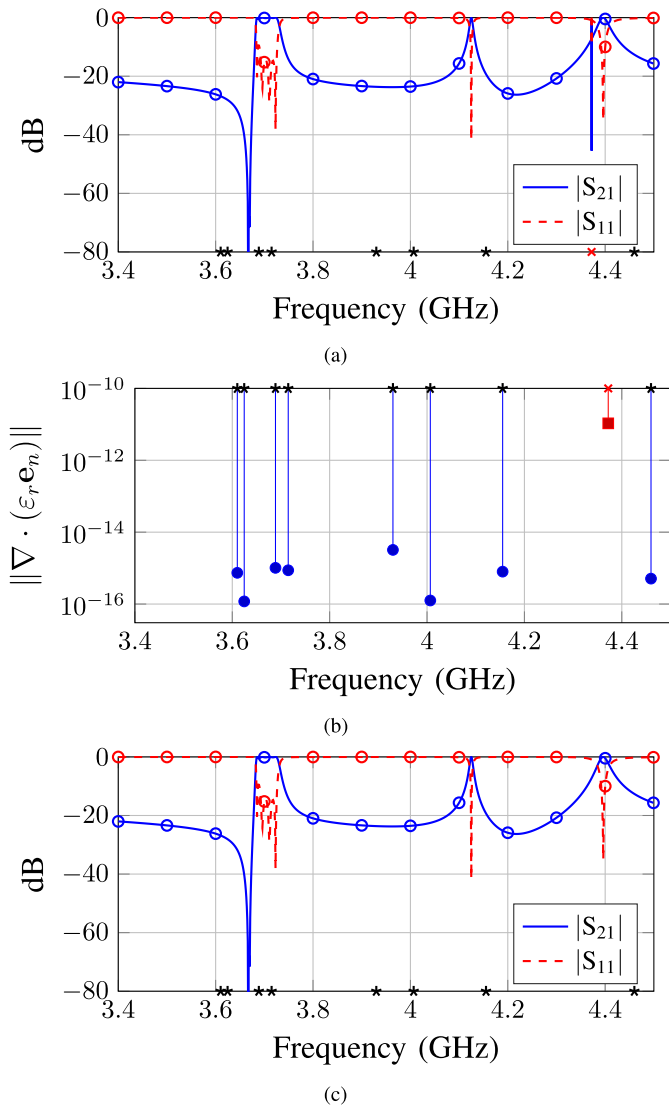
(a)

(b)

(c)

Fig. 4. Quad-mode dielectric resonator filter response. (–) RBM. (o) FEM. (a) Spurious mode contribution. Note the spike around 4.372 GHz, highlighted with a red cross on the frequency axis. (b) In-band mode divergence norm $\|\nabla \cdot (\varepsilon_r \mathbf{e}_n)\|$. (c) Free of spurious mode contribution. Note there is no longer a spike around 4.372 GHz.
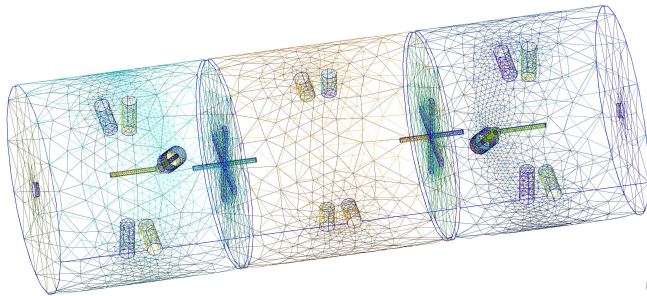

Fig. 5. Triple-band filter in elliptical cavities designed in [55].
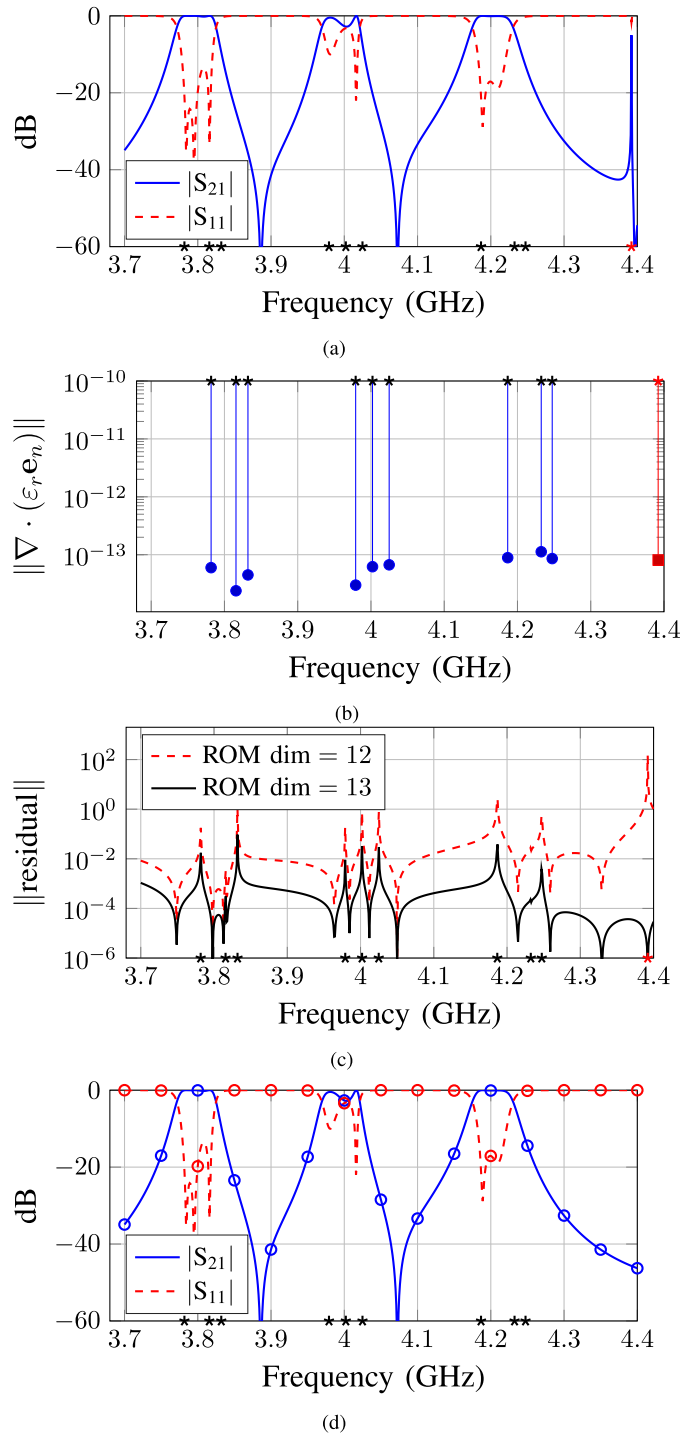

(a)

(b)

(c)

(d)

Fig. 6. Triple-band filter response. (–) RBM. (o) FEM. (a) Possible spurious mode contribution. ROM dimension = 12. Note the spike around 4.392 GHz, highlighted with a red cross on the frequency axis. (b) In-band mode divergence norm $\|\nabla \cdot (\varepsilon_r \mathbf{e}_n)\|$. (c) Residual norm in the ROM. (d) ROM dimension = 13.

well along the frequency axis. Taking a closer look at both Fig. 6(a) and (d), we identify a spike on the frequency response in Fig. 6(a). In addition, there is an in-band mode around this spike at 4.392 GHz. We could have straight away identified this spike as a spurious mode contribution due to the in-band

mode at 4.392 GHz, which can then be characterized as a spurious mode. This reasoning would be plausible. However, when we carry out the variational divergence analysis for each of the in-band modes, detailed in Fig. 6(b), we realize this spike is due to a divergence-free contribution, just like the other in-band modes and, therefore, it is *not* a spurious mode. This contribution should *not* be removed from the

This article has been accepted for inclusion in a future issue of this journal. Content is final as presented, with the exception of pagination.

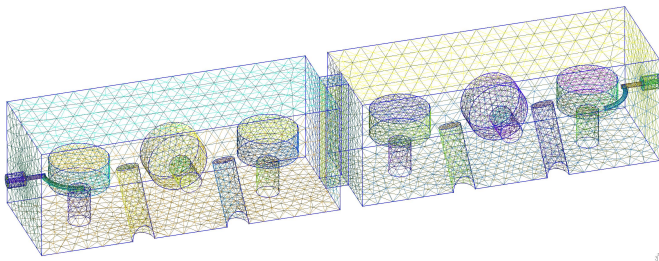DE LA RUBIA *et al.*: SPURIOUS MODES IN MOR IN VARIATIONAL PROBLEMS

11

Fig. 7.   Inline dielectric resonator filter designed in [56].

ROM, since this is indeed a physical contribution. If we do so, we will definitely deteriorate the approximation capabilities in MOR in electromagnetics. What is going on with this spike is the following. This in-band mode is the result of a poorly approximated higher-order physical mode in the structure, which is out of the band of analysis, but due to the poor approximation at this step in the MOR, this higher-order mode shows up in the band of analysis. This is already clear in the residual behavior of the ROM, shown in Fig. 6(c). In the case of the ROM of dimension 12, the residual norm of the ROM $\|r(\tilde{\mathbf{E}}(k), \cdot; k)\|_{\mathcal{H}'}$ is still large nearby 4.392 GHz, which clearly identifies a poor ROM approximation around this frequency. Indeed, following the greedy procedure detailed in Algorithm 1, the reduced-basis space will be enriched by a snapshot of the electric field at this frequency 4.392 GHz, giving rise to a ROM of dimension 13, where this poor approximated higher order mode is pushed away to its right place out of the band of analysis $\mathcal{B}$. This is shown in both the residual norm for the ROM of dimension 13 and the scattering parameter results in Fig. 6(c) and (d), respectively. It should be noted that this possible spurious mode, which turned out to be a physical mode, is no longer present in Fig. 6(d) following Algorithm 1.

C. Inline Dielectric Resonator Filter

A sixth-order inline dielectric resonator filter with two transmission zeros is depicted in Fig. 7. Cross-coupling between nonadjacent dielectric resonators, appropriately arranging their orientations, is obtained by exploiting multiple evanescent modes in the inline structure. This filter is proposed in [56]. The [2.15, 2.19] GHz band is taken into account for analysis. An FEM discretization shown in Fig. 7 with 229 706 degrees of freedom is used. Following Algorithm 1, a ROM is obtained giving rise to a reduced system of dimension 11 to compute the fast frequency sweep detailed in Fig. 8(a). It should be pointed out that all steps in Algorithm 1 are run until the final dimension 11 is obtained to ensure the convergence of the ROM. No spurious mode was previously identified in this process. The comparison between the FEM and MOR results is depicted in Fig. 8 as well and good agreement is found. The in-band modes found in the band of analysis are also detailed along the frequency axis in Fig. 8(a). We find a spike in the scattering parameter response around 2.176 GHz. We carry out the variational divergence analysis for each of the in-band modes, shown in Fig. 8(b), and we realize this spike is due to a spurious mode solution, that is, a nonphysical
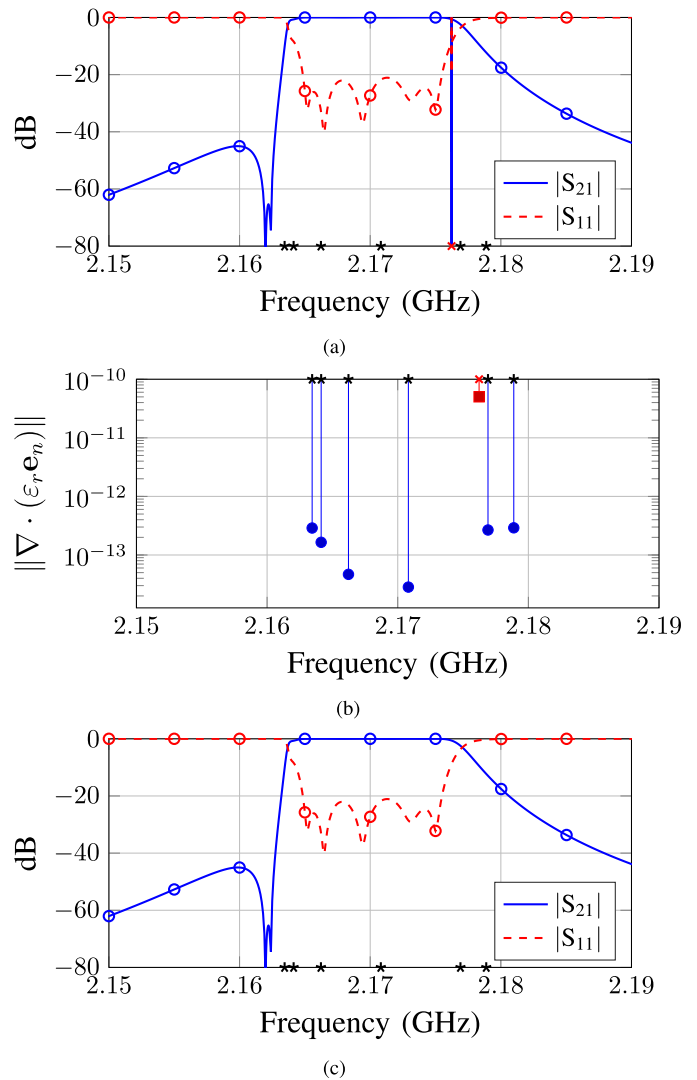

Fig. 8.   Inline dielectric resonator filter with finite transmission zeros response. (–) RBM. (○) FEM. (a) Spurious mode contribution. Note the spike around 2.176 GHz, highlighted with a red cross on the frequency axis. (b) In-band mode divergence norm $\|\nabla \cdot (\varepsilon_r \mathbf{e}_n)\|$. (c) Free of spurious mode contribution.

mode, since it does not show a divergence-free contribution as can be observed in the remaining in-band modes. As a result, this spurious mode contribution should be filtered out from the device response. All this is taken into account in Algorithm 1. Here, we are just highlighting step by step the proposed approach detailed in Algorithm 1. As a result, no spike is observed in the scattering parameter response since any spurious mode contribution has been removed in Fig. 8(c). It should be pointed out that, following Algorithm 1, only physical in-band mode contributions are allowed in the final reliable ROM response shown in Fig. 8(c).

V. CONCLUSION

A robust reduced-order model for reliable fast frequency sweep in microwave circuits has been detailed. We have addressed the everlasting issue of poorly localized approximation problems in MOR in electromagnetics and spurious modes have been identified for the very first time in ROMs for time-harmonic Maxwell's equations. A computational inexpensive

variational divergence condition has been proposed to identify nonphysical spurious modes in the band of analysis since any in-band physical mode must be divergence-free. An algorithm has been detailed to completely remove any spurious mode contribution from the ROM, without having to enrich the actual reduced-basis approximation space in the MOR process. This filtering strategy has been based upon physical coupling to in-band mode arguments. It has to be pointed out that, in the proposed approach, when a spurious mode is identified, not only the ROM response itself has been regularized but also the corresponding error estimator behavior has been unleashed from any spurious mode contribution. This has allowed the MOR process to keep going smoothly without any stagnation. Actual microwave devices, including a quad-mode filter, a triple-band filter, and an inline filter with finite transmission zeros, have shown the capabilities and reliability of the proposed methodology.

Spurious modes are mathematical solutions that are non-physical solutions to the physical problem under consideration. In electromagnetics, we may think the curl equations (Ampère's and Faraday's laws) are enough to satisfy *all* Maxwell's equations, provided the frequency does not vanish. However, in MOR, this is not enough since we have shown that the divergence-free equation is no longer satisfied in the ROM, giving rise to spurious solutions. As a result, any CEM problem suffers from spurious solutions whenever standard MOR techniques are taken into account. We have shown some filtering structures in this work, as typical examples of cavity problems in electromagnetics. But this spurious mode issue also appears in other electromagnetic problems, such as diplexers, electromagnetic bandgaps, frequency selective surfaces, power dividers, and so on. Any cavity problem in electromagnetics will suffer from these spurious modes when standard MOR techniques are used.

By the same token, in open problems, such as radiation problems, spurious modes in MOR may show up, since the divergence-free equation is not appropriately satisfied. However, in these open electromagnetic problems, the resonances are no longer found on the frequency axis but are away from the frequency axis. In this scenario, even though the MOR may suffer from spurious modes, these will not be noted along the frequency axis.

References

[1] A. Bossavit, *Computational Electromagnetism: Variational Formulations, Complementarity, Edge Elements*. New York, NY, USA: Academic, 1998.

[2] J.-C. Nédélec, "Mixed finite elements in $\mathbb{R}^3$," *Numer. Math.*, vol. 35, no. 3, pp. 315–341, 1980.

[3] J. C. Nedelec, "A new family of mixed finite elements in $\mathbb{R}^3$," *Numer. Math.*, vol. 50, no. 1, pp. 57–81, May 1986.

[4] A. Bossavit, "Solving Maxwell equations in a closed cavity, and the question of 'spurious modes,'" *IEEE Trans. Magn.*, vol. 26, no. 2, pp. 702–705, Mar. 1990.

[5] J. P. Webb, "Edge elements and what they can do for you," *IEEE Trans. Magn.*, vol. 29, no. 2, pp. 1460–1465, Mar. 1993.

[6] J. P. Webb, "Hierarchal vector basis functions of arbitrary order for triangular and tetrahedral finite elements," *IEEE Trans. Antennas Propag.*, vol. 47, no. 8, pp. 1244–1253, Aug. 1999.

[7] S.-C. Lee, J.-F. Lee, and R. Lee, "Hierarchical vector finite elements for analyzing waveguiding structures," *IEEE Trans. Microw. Theory Techn.*, vol. 51, no. 8, pp. 1897–1905, Aug. 2003.

[8] Y. Konkel, O. Farle, A. Sommer, S. Burgard, and R. Dyczij-Edlinger, "A posteriori error bounds for Krylov-based fast frequency sweeps of finite-element systems," *IEEE Trans. Magn.*, vol. 50, no. 2, pp. 441–444, Feb. 2014.

[9] J. L. Nicolini, D.-Y. Na, and F. L. Teixeira, "Model order reduction of electromagnetic particle-in-cell kinetic plasma simulations via proper orthogonal decomposition," *IEEE Trans. Plasma Sci.*, vol. 47, no. 12, pp. 5239–5250, Dec. 2019.

[10] A. Hochman, J. F. Villena, A. G. Polimeridis, L. M. Silveira, J. K. White, and L. Daniel, "Reduced-order models for electromagnetic scattering problems," *IEEE Trans. Antennas Propag.*, vol. 62, no. 6, pp. 3150–3162, Jun. 2014.

[11] M. Rewienski, A. Lamecki, and M. Mrozowski, "Greedy multipoint model-order reduction technique for fast computation of scattering parameters of electromagnetic systems," *IEEE Trans. Microw. Theory Techn.*, vol. 64, no. 6, pp. 1681–1693, Jun. 2016.

[12] L. Codecasa, G. G. Gentili, and M. Politi, "Exploiting port responses for wideband analysis of multimode lossless devices," *IEEE Trans. Microw. Theory Tech.*, vol. 68, no. 2, pp. 555–563, Feb. 2020.

[13] Q. I. Dai, Y. H. Lo, W. C. Chew, Y. G. Liu, and L. Jiang, "Generalized modal expansion and reduced modal representation of 3-D electromagnetic fields," *IEEE Trans. Antennas Propag.*, vol. 62, no. 2, pp. 783–793, Feb. 2014.

[14] L. Xue and D. Jiao, "Rapid modeling and simulation of integrated circuit layout in both frequency and time domains from the perspective of inverse," *IEEE Trans. Microw. Theory Tech.*, vol. 68, no. 4, pp. 1270–1283, Apr. 2020.

[15] L. Balewski *et al.*, "Step on it bringing fullwave finite-element microwave filter design up to speed," *IEEE Microw. Mag.*, vol. 21, no. 3, pp. 34–49, Mar. 2020.

[16] D. Szypulski, G. Fotyga, V. de la Rubia, and M. Mrozowski, "A subspace-splitting moment-matching model-order reduction technique for fast wideband FEM simulations of microwave structures," *IEEE Trans. Microw. Theory Tech.*, vol. 68, no. 8, pp. 3229–3241, Aug. 2020.

[17] A. Monje-Real and V. de la Rubia, "Electric field integral equation fast frequency sweep for scattering of nonpenetrable objects via the reduced-basis method," *IEEE Trans. Antennas Propag.*, vol. 68, no. 8, pp. 6232–6244, Aug. 2020.

[18] M. Mul, V. de la Rubia, G. Fotyga, A. Lamecki, and M. Mrozowski, "Regularized local multivariate reduced-order models with nonaffine parameter dependence," *IEEE Trans. Microw. Theory Tech.*, vol. 67, no. 5, pp. 1778–1789, May 2019.

[19] Y. Zhu and A. C. Cangellaris, "Robust finite-element solution of lossy and unbounded electromagnetic eigenvalue problems," *IEEE Trans. Microw. Theory Techn.*, vol. 50, no. 10, pp. 2331–2338, Oct. 2002.

[20] M. Kordy, E. Cherkaev, and P. Wannamaker, "Adaptive model order reduction for the Jacobian calculation in inverse multi-frequency problem for Maxwell's equations," *Appl. Numer. Math.*, vol. 109, pp. 1–18, Nov. 2016.

[21] M. Kordy, E. Cherkaev, and P. Wannamaker, "Null space correction and adaptive model order reduction in multi-frequency Maxwell's problem," *Adv. Comput. Math.*, vol. 43, no. 1, pp. 171–193, 2017.

[22] V. de la Rubia, "Description of microwave circuits via the reduced-basis method giving physical insight," *IEEE Trans. Antennas Propag.*, early access, Sep. 20, 2022, doi: 10.1109/TAP.2022.3206536.

[23] F. Ballarin, A. Manzoni, A. Quarteroni, and G. Rozza, "Supremizer stabilization of POD–Galerkin approximation of parametrized steady incompressible Navier–Stokes equations," *Int. J. Numer. Methods Eng.*, vol. 102, no. 5, pp. 1136–1161, 2015.

[24] A. E. Løvgren, Y. Maday, and E. M. Rønquist, "A reduced basis element method for the steady Stokes problem," *ESAIM, Math. Model. Numer. Anal.*, vol. 40, no. 3, pp. 529–552, 2006.

[25] E. Fonn, H. van Brummelen, T. Kvamsdal, and A. Rasheed, "Fast divergence-conforming reduced basis methods for steady Navier–Stokes flow," *Comput. Methods Appl. Mech. Eng.*, vol. 346, pp. 486–512, Apr. 2019.

[26] V. Girault and P.-A. Raviart, *Finite Element Methods for Navier-Stokes Equations*. Berlin, Germany: Springer-Verlag, 1986.

[27] P. Monk, *Finite Element Methods for Maxwell's Equations*. New York, NY, USA: Oxford Univ. Press, 2003.

[28] A. Kirsch and F. Hettlich, *The Mathematical Theory of Time-Harmonic Maxwell's Equations*. Cham, Switzerland: Springer, 2015.

[29] V. de la Rubia and M. Mrozowski, "A compact basis for reliable fast frequency sweep via the reduced-basis method," *IEEE Trans. Microw. Theory Techn.*, vol. 66, no. 10, pp. 4367–4382, Oct. 2018.

This article has been accepted for inclusion in a future issue of this journal. Content is final as presented, with the exception of pagination.

DE LA RUBIA *et al.*: SPURIOUS MODES IN MOR IN VARIATIONAL PROBLEMS

13

[30] K. Kurokawa, *An Introduction to the Theory of Microwave Circuits*. New York, NY, USA: Academic, 1969.

[31] G. Conciauro, M. Guglielmi, and R. Sorrentino, *Advanced Modal Analysis*. New York, NY, USA: Wiley, 2000.

[32] J. Zhu and D. Jiao, "A theoretically rigorous full-wave finite-element-based solution of Maxwell's equations from DC to high frequencies," *IEEE Trans. Adv. Packag.*, vol. 33, no. 4, pp. 1043–1050, Nov. 2010.

[33] R. J. Cameron, C. M. Kudsia, and R. R. Mansour, *Microwave Filters for Communication Systems: Fundamentals, Design, and Applications*. Hoboken, NJ, USA: Wiley, 2018.

[34] A. T. Patera and G. Rozza, *Reduced Basis Approximation and a Posteriori Error Estimation for Parametrized Partial Differential Equations*. Cambridge, MA, USA: MIT Press, 2007.

[35] P. Benner, K. Willcox, and S. Gugercin, "A survey of projection-based model reduction methods for parametric dynamical systems," *SIAM J. Sci. Comput.*, vol. 57, no. 4, pp. 483–531, 2015.

[36] A. Quarteroni, A. Manzoni, and F. Negri, *Reduced Basis Methods for Partial Differential Equations*. Cham, Switzerland: Springer, 2016.

[37] J. S. Hesthaven, G. Rozza, and B. Stamm, *Certified Reduced Basis Methods for Parametrized Partial Differential Equations*. Berlin, Germany: Springer, 2016.

[38] L. Feng and P. Benner, "A new error estimator for reduced-order modeling of linear parametric systems," *IEEE Trans. Microw. Theory Tech.*, vol. 67, no. 12, pp. 4848–4859, Dec. 2019.

[39] L. Feng, A. C. Antoulas, and P. Benner, "Some *a posteriori* error bounds for reduced-order modelling of (non-) parametrized linear systems," *ESAIM, Math. Model. Numer. Anal.*, vol. 51, no. 6, pp. 2127–2158, 2017.

[40] A. Sommer, O. Farle, and R. Dyczij-Edlinger, "Certified dual-corrected radiation patterns of phased antenna arrays by offline–online order reduction of finite-element models," *J. Comput. Phys.*, vol. 299, pp. 22–44, Oct. 2015.

[41] M. W. Hess, S. Grundel, and P. Benner, "Estimating the inf-sup constant in reduced basis methods for time-harmonic Maxwell's equations," *IEEE Trans. Microw. Theory Techn.*, vol. 63, no. 11, pp. 3549–3557, Nov. 2015.

[42] M. Rewieński, A. Lamecki, and M. Mrozowski, "A goal-oriented error estimator for reduced basis method modeling of microwave devices," *IEEE Microw. Wireless Compon. Lett.*, vol. 25, no. 4, pp. 208–210, Apr. 2015.

[43] R. Baltes, A. Schultschik, O. Farle, and R. Dyczij-Edlinger, "A finite-element-based fast frequency sweep framework including excitation by frequency-dependent waveguide mode patterns," *IEEE Trans. Microw. Theory Techn.*, vol. 65, no. 7, pp. 2249–2260, Jul. 2017.

[44] V. de la Rubia, U. Razafison, and Y. Maday, "Reliable fast frequency sweep for microwave devices via the reduced-basis method," *IEEE Trans. Microw. Theory Techn.*, vol. 57, no. 12, pp. 2923–2937, Dec. 2009.

[45] M. W. Hess and P. Benner, "Fast evaluation of time–harmonic Maxwell's equations using the reduced basis method," *IEEE Trans. Microw. Theory Techn.*, vol. 61, no. 6, pp. 2265–2274, Jun. 2013.

[46] G. Fotyga, M. Czarniewska, A. Lamecki, and M. Mrozowski, "Reliable greedy multipoint model-order reduction techniques for finite-element analysis," *IEEE Antennas Wireless Propag. Lett.*, vol. 17, no. 5, pp. 821–824, May 2018.

[47] W. Wang, G. N. Paraschos, and M. N. Vouvakis, "Fast frequency sweep of FEM models via the balanced truncation proper orthogonal decomposition," *IEEE Trans. Antennas Propag.*, vol. 59, no. 11, pp. 4142–4154, Nov. 2011.

[48] R. Wang, D. J. Riley, and J.-M. Jin, "Application of tree-cotree splitting to the time-domain finite-element analysis of electromagnetic problems," *IEEE Trans. Antennas Propag.*, vol. 58, no. 5, pp. 1590–1600, May 2010.

[49] V. de la Rubia, "Reliable reduced-order model for fast frequency sweep in microwave circuits," *Electromagnetics*, vol. 34, nos. 3–4, pp. 161–170, 2014.

[50] H. Brezis, *Functional Analysis, Sobolev Spaces and Partial Differential Equations*. New York, NY, USA: Springer, 2011.

[51] V. de la Rubia, "Physics-based greedy algorithm for reliable fast frequency sweep in electromagnetics via the reduced-basis method," *IEEE Trans. Antennas Propag.*, early access, Sep. 20, 2022, doi: 10.1109/TAP.2022.3206544.

[52] P. Ingelstrom, "A new set of H(curl)-conforming hierarchical basis functions for tetrahedral meshes," *IEEE Trans. Microw. Theory Tech.*, vol. 54, no. 1, pp. 106–114, Jan. 2006.

[53] C. Geuzaine and J.-F. Remacle, "Gmsh: A 3-D finite element mesh generator with built-in pre- and post-processing facilities," *Int. J. Numer. Methods Eng.*, vol. 79, no. 11, pp. 1309–1331, 2009.

[54] M. Memarian and R. R. Mansour, "Quad-mode and dual-mode dielectric resonator filters," *IEEE Trans. Microw. Theory Techn.*, vol. 57, no. 12, pp. 3418–3426, Dec. 2009.

[55] L. Zhu, R. R. Mansour, and M. Yu, "Triple-band cavity bandpass filters," *IEEE Trans. Microw. Theory Techn.*, vol. 66, no. 9, pp. 4057–4069, Sep. 2018.

[56] S. Bastioli and R. V. Snyder, "Inline pseudoelliptic $TE_{01\delta}$-mode dielectric resonator filters using multiple evanescent modes to selectively bypass orthogonal resonators," *IEEE Trans. Microw. Theory Tech.*, vol. 60, no. 12, pp. 3988–4001, Dec. 2012.

Valentín de la Rubia received the Ingeniero de Telecomunicación and Ph.D. degrees from the Universidad Politécnica de Madrid, Madrid, Spain, in 2003 and 2008, respectively.

He has been an Assistant Professor with the Universidad Politécnica de Madrid since 2011. His current research interests include CEM and model-order reduction techniques, such as RBMs, for fast and reliable electromagnetic (EM) analysis, placing special emphasis on the development of EM-based computer-aided design (CAD) tools.

David Young, photograph and biography not available at the time of publication.

Grzegorz Fotyga (Member, IEEE) received the M.S.E.E. and Ph.D. degrees in electronic engineering from the Gdańsk University of Technology, Gdańsk, Poland, in 2009 and 2016, respectively.

He is currently an Assistant Professor with the Department of Microwave and Antenna Engineering, Gdańsk University of Technology. His current research interests include CEM, numerical methods, finite-element methods, and model-order reduction.

Michal Mrozowski (Fellow, IEEE) received the M.Sc. and Ph.D. degrees from the Gdańsk University of Technology, Gdańsk, Poland, in 1983 and 1990, respectively.

In 1986, he joined the Faculty of Electronics, Gdańsk University of Technology, where he is currently a Full Professor and the Head of the Department of Microwave and Antenna Engineering. His research interests include CEM, GPU computing, computer-aided design (CAD) of microwave devices, filter design, and optimization techniques.